Origin and Potential Geothermal Significance of China Hat and Other Late Pleistocene Topaz Rhyolite Lava Domes of the Blackfoot Volcanic Field, SE Idaho

Michael McCurry[1], David M. Pearson[1], John Welhan[2], Shannon K. Natwotniak[1], and Meghan Fisher[1]

[1]Department of Geosciences, Idaho State University, Pocatello, ID
[2]Idaho Geological Survey, University of Idaho, Moscow, ID

Keywords

Magma-related, rhyolite, Snake River Plain, Idaho, blind geothermal systems, Quaternary tectonics

ABSTRACT

The Snake River Plain and neighboring regions are well known for their high heat flow and robust Neogene-Quaternary tectonic and magmatic activity. Interestingly, however, there are comparatively few surficial manifestations of geothermal activity. This study is part of a renewed examination of this region as a possible hidden or blind geothermal resource. We present an integrated conceptual model for basalts and genetically derivative topaz rhyolite lava domes of the Blackfoot Volcanic Field (BVF), linking ultimate heat and mass sources rooted in the upper mantle to potential blind geothermal systems in the upper crust. In our model intracrustal magma transfer and storage respond opportunistically and interactively evolving tectonic processes. Production of rhyolite magma is dominated by mantle-derived mass and heat sources. Rhyolite formation processes via fractional crystallization, cyclic remelting, mixing and assimilation occur mainly in the mid- to upper-crust, contributing to incremental assembly of an evolving magma storage and pluton system. Pre-eruption storage and phenocryst formation for China Hat occurred at ~14 km depth, and is inferred to be representative of the most evolved parts of the magmatic system. Approximately 1.2 km^3 of topaz rhyolite have been erupted since 1.6 Ma and up to another 350 km^3 of silicic rocks may have been intruded as hypabyssal dikes and sills at depths of 0.5 to 6 km. Average silicic magma production rate could therefore be on the order of ~1 to 200 km^3/m.y. Given simple assumptions of magma genesis, eruption rates, and initial and final volatile concentrations, we infer average H_2O and CO_2 volatile fluxes from the rhyolite source region of ~0.1 to 10 MT/year and 10 to 1000 T/day, respectively. Lithium flux may be comparable to CO_2, and it may be both an effective tracer and resource in fluids derived from the inferred consolidating China Hat magma body.

Introduction

There is significant renewed interest in the geothermal potential of Idaho along and adjacent to the Yellowstone-Snake River Plain hot spot track (YSRP) as reflected in numerous recent publications (e.g., McLing et al. 2014; Podgorney et al. 2013; Welhan et al. 2014; McCurry and Welhan 2012). Recent research derives in part from renewed interest in EGS systems (DOE FORGE), for which the area is well known (e.g., Tester et al. 2006), and from recent studies indicating a potential for the existence of hidden or blind high-temperature geothermal systems in the region associated with young rhyolite volcanoes (e.g., Welhan et al., 2014; McCurry and Welhan, 2012).

This paper focuses on the Quaternary Blackfoot Volcanic Field (BVF, Figure 1). This field is well suited for analysis as a blind resource because of its distinctive combination of (1) young bimodal volcanism (e.g., Fiesinger et al. 1982), petrogenetic evidence of shallow magma storage and evolution (e.g., Ford 2005), presence of coeval extension (e.g., Polun 2011), voluminous thermogenic travertine deposits (e.g., Ohly, ISU MS Thesis in prep.), and C- and He-isotopic evidence of active magma degassing (Lewicki et al. 2013); (2) a paucity of hot springs or other obvious indicators of

a geothermal resource in the immediate vicinity of the lava domes (e.g., Autenrieth et al. 2011); and (3) proximity to a region of high crustal heat flow, high-T geothermal fluids at 2.5-5 km depth and micro-seismicity characterized by its swarming nature (e.g., Welhan et al., 2014).

The BVF is the largest and youngest bimodal volcanic field located close to but offset slightly from YSRP. Quaternary 'topaz rhyolite' lava domes, including 57 ka China Hat dome field, dot the central parts of BVF. Early geothermal assessments of BVF noted favorable characteristics of the region for geothermal potential such as young and robust bimodal volcanism, gravity and magnetic field anomalies, recent and active tectonic extension, spring activity, high regional heat flow and abundant travertine, but also noted paucity of key features associated with shallow high-T hydrothermal activity and potential (e.g., Mitchell 1976; Hutsinpiller and Parry, 1984). Industry based estimates of significant geothermal power potential are summarized by Neely and Galinato (2007), however these have not yet led to development or production of geothermal energy. More recent work has focused on the region as a magmatically-related (e.g., Arehart et al., 2002), blind ('hidden') or EGS geothermal resource (e.g., Welhan et al. 2014; McCurry and Welhan 2012; and references therein). Interestingly, renewed examination of regional spring waters have yielded He and C-isotope gas chemistry and fluxes comparable to quiescent volcanoes (Lewicki et al., 2013).

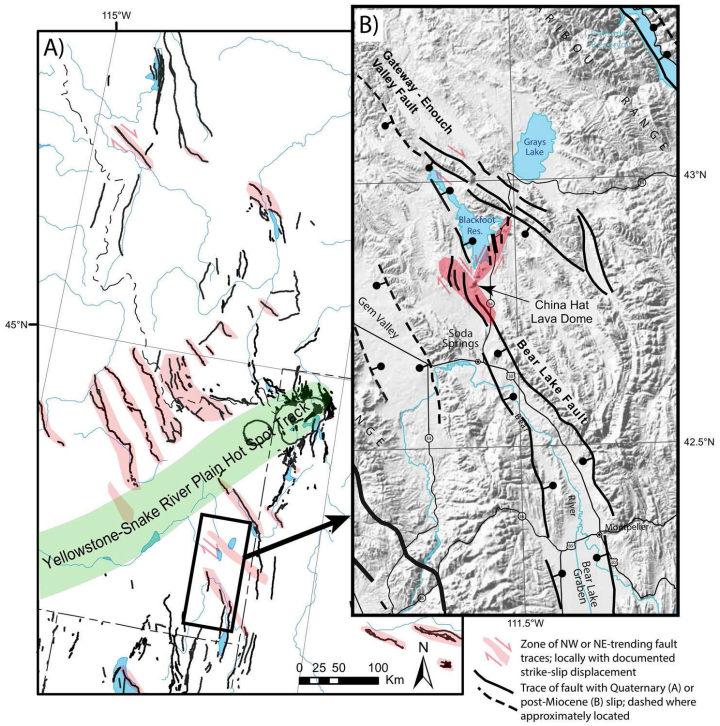

Figure 1. Location and regional tectonic setting of China Hat and the Blackfoot Volcanic Field. A) Faults with documented Quaternary activity (modified from U.S. Geological Survey, http://earthquake.usgs.gov/hazards/qfaults/map/), highlighted abundant northwest trending structural grain interpreted here to reflect reactivation of a pre-existing fabric. B) Inset showing faults with documented post-Miocene displacement (modified from Breckenridge et al., 2003), *en-echelon* conjugate faulting near Blackfoot Reservoir and the northwestward transition from predominantly north-south structures to northwest-striking structures.

Our principle objective is to use existing information to extend and improve conceptual models for BVF (e.g., Autenrieth et al. 2011; McCurry and Welhan 2012; Welhan et al. 2014) as a basis for future research. Our model links ultimate heat and mass sources, pathways and processes, to shallow, potentially geothermally accessible regions in an adaptable and testable fashion. We frame our conceptual model on the basis of geologic, geophysical and geochemical context for BVF. In this preliminary phase of model development we emphasize the tectonic, volcanic and magmatic context for deeper parts of the system. We reassesses and extend the possible range of genetic relationships between faults which overlap in time and space with BVF rhyolites, and their implications for Quaternary tectonic processes and magmatism. We present a conceptual model of magma petrogenesis that provides a preliminary framework for testing the idea that significant heat currently resides in mid- to upper crustal regions in a association with this magmatic system (e.g., McCurry and Welhan, 2012). We also assess the plausibility that the rhyolite magmatic system contributes traceable and potentially valuable solutes and heat (e.g., lithium, carbon and ^{3}He) to shallower hydrothermal and groundwater systems. Lastly, we propose future types of work that we believe would lead to better assessment of the geothermal potential of the area.

Tectonic Context and Implications for Magmatism

The Blackfoot volcanic field (BVF) is located within the Intermountain seismic belt, the primary region of seismicity and active extension at the eastern border of the northern Basin and Range (Smith and Sbar, 1974). The north-south trending Intermountain seismic belt is generally characterized by west-dipping faults in Utah, which transitions to a predominantly northwest-trending structural grain in east-central Idaho and southwestern Montana (Fig. 1), consistent with the regional transition in GPS-derived extension direction (Payne et al., 2012). This mimics pre-existing fold-thrust belt structure near the northern boundary of the Wyoming salient; several major individual Basin and Range normal faults clearly inverted pre-existing fold-thrust belt structures in eastern Idaho and western Wyoming near the northern boundary of the Wyoming salient (Royse et al., 1975).

BVF occurs at the transition to northwest-striking structures that dominate east-central Idaho (Fig. 1B). Near Blackfoot Reservoir, normal faults cut basin-filling basalt and form fault sets with two discrete orientations (Fig. 1B; Polun, 2011): 1) west-northwest striking faults within the Willow Creek lava field and similarly oriented left stepping

en-echelon faults at the southwestern margin of Blackfoot Reservoir; these faults define northwest-trending zones that accommodate dextral oblique extension: 2) right-stepping faults that form a northeasterly trend at the eastern margin of Blackfoot Reservoir and are consistent with sinistral oblique extension. Similar right-stepping north to northeast-striking faults were previously observed along the trace of the Teton fault to the northeast of Blackfoot Reservoir (Byrd and Smith, 1994) and may reflect sinistral strike-slip displacement of the southeastern margin of the Snake River Plain (Payne et al., 2012). The 60-70° angle between the two sets of structures is consistent with conjugate faulting that accommodates north-south shortening and east-west extension.

The lack of prominent faults, an absence of seismicity, and the association of basaltic dikes with young systems of normal faults within the Snake River Plain were used to suggest a temporal shift from tectonic extension to active dike intrusion that keeps pace with extension in the adjacent Basin and Range (Rodgers et al., 2002). Within the Blackfoot volcanic field, prominent *en echelon* normal faults occur in the interior of the basin as opposed to at the range boundaries and yield higher strain rates than surrounding Basin and Range structures, taken as evidence that these structures represent the surface expressions of dike injection that are thought to be analogous to "volcanic rifts" within the Snake River Plain (Polun, 2011; Fig. 1). However, abundant historical seismicity beneath the eastern Blackfoot volcanic field (Welhan et al., 2014) suggests that faults there may not be analogous to aseismic volcanic rifts within the Snake River Plain. Additionally, recent GPS results from the northern Basin and Range yield a negligible rate of extension within the eastern Snake River Plain, suggesting the strengthened crust there does not accommodate significant extension, even by dike injection, calling into question the role of magmatism in driving or keeping pace with normal faulting at the surface in this region (Payne et al., 2012). The relative timing of late Pleistocene magmatism within the Blackfoot volcanic field, compared to primarily ~10-4 Ma magmatism in the adjacent Snake River Plain (Pierce and Morgan, 1992), also supports a tectonic origin for normal faults within the Blackfoot volcanic field because it provides a mechanism for continual magma transfer that postdates that within the adjacent Snake River Plain (McCurry and Welhan, 2012).

In agreement with Polun (2011), we also emphasize an important interplay between magmatism and surface faulting in the Blackfoot volcanic field. However, we suggest a second, alternative hypothesis involving a primary tectonic control for the structural setting of the Blackfoot volcanic field and associated late Pleistocene magmatism. We suggest that Basin and Range extension reactivated a previous northwest-trending structural grain in eastern and east-central Idaho within the northern margin of the Wyoming salient, resulting in oblique dextral extension along northwest-striking normal faults (Fig. 1). In addition, a conjugate north-northeast striking fault set accommodates oblique-sinistral extension parallel to the eastern margin of the Snake River Plain and rigid southwestward displacement relative to the adjacent Basin and Range (Payne et al., 2012). Together, these fault systems accommodate east-west extension, and in Blackfoot volcanic field set up dilational fault intersections that may result in continued generation and storage of magma in the lower and middle crust. Conjugate faulting of this orientation is not unique to this portion of the Basin and Range and is also documented in the Eastern California shear zone-Walker Lane of eastern California and Nevada (Faulds and Henry, 2008). These structural settings are considered some of the most favorable for geothermal systems because they create pathways for fluid and melt migration (Faulds et al., 2011). Consideration of the Blackfoot volcanic field as primarily a result of Basin and Range tectonism would represent a significant departure from prior work (e.g., Polun, 2011), and distinguishing these hypotheses would be an important goal of future research. We speculate that, analogous to en echelon normal fault traces in Iceland (Grant and Kattenhorn, 2004), oblique extension is also occurring in the BVF as a consequence of the transition in extension direction (Payne et al., 2012). These structures may have facilitated formation of steeply-dipping crustal conduits that enable magma transfer adjacent to the eastern Snake River Plain. Structural controls on magma emplacement may therefore play a fundamental role in magma transfer, storage and emplacement and size of a shallow high-T geothermal resource associated with this volcanic system.

Volcanic Context

The BVF is a basalt-dominated, bimodal volcanic field (Fiesinger et al., 1982; Pickett 2004; Ford 2005). Eruptions of primitive to moderately evolved olivine tholeiite lavas, compositionally and mineralogically similar to those of ESRP (Pickett 2004; McCurry et al. 2008), occurred from widely scattered vents over an area of 1375 km^2, extending ~30 to 80 km southeast of ESRP and YSRP (Figure 2). A cumulative volume of ~100 km^3 of lavas partially infill several late Miocene to late Quaternary Basin and Range grabens to maximum depths of at least 230 m (Welhan et al., 2014). Effusive and minor phreatomagmatic basalt eruptions occurred between at least 1.5 Ma and ~30 ka (Luedke et al., 1983; Pickett, 2004). Fiesinger et al. (1982) and Pickett (2004) note apparent alignments of basalt vents with Neogene-Quaternary normal faults, and that mutual cross-cutting relationships indicate overlap in age of faulting and volcanism.

Rhyolite Lava Domes

Three clusters of rhyolite lava domes dot the center of the BVF field (Figure 2, 3). Northern and central (Sheep Island) dome fields yield overlapping K/Ar dates of 1.59±0.06 and 1.41±15 Ma, respectively (dates compiled by Luedke and Smith,

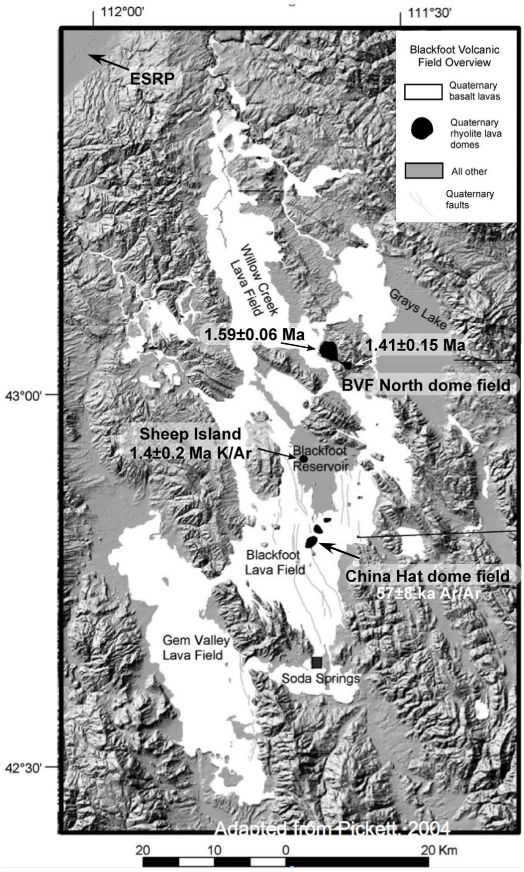

Figure 2. Volcanic rocks of the Blackfoot Volcanic Field. White color indicates Quaternary basalt lava plains covered by thin, discontinuous layer or late Pleistocene to Holocene loess. Black color illustrates locations of rhyolite lava domes. Light grey lines crossing the basalt plains are representative of numerous small late Pleistocene dike-related and, or tectonic-faults (cf. Figure 1). Dark grey patterns indicate other undifferentiated rock types, mostly late Proterozoic to Mesozoic sedimentary rocks of the Sevier fold and thrust belt.

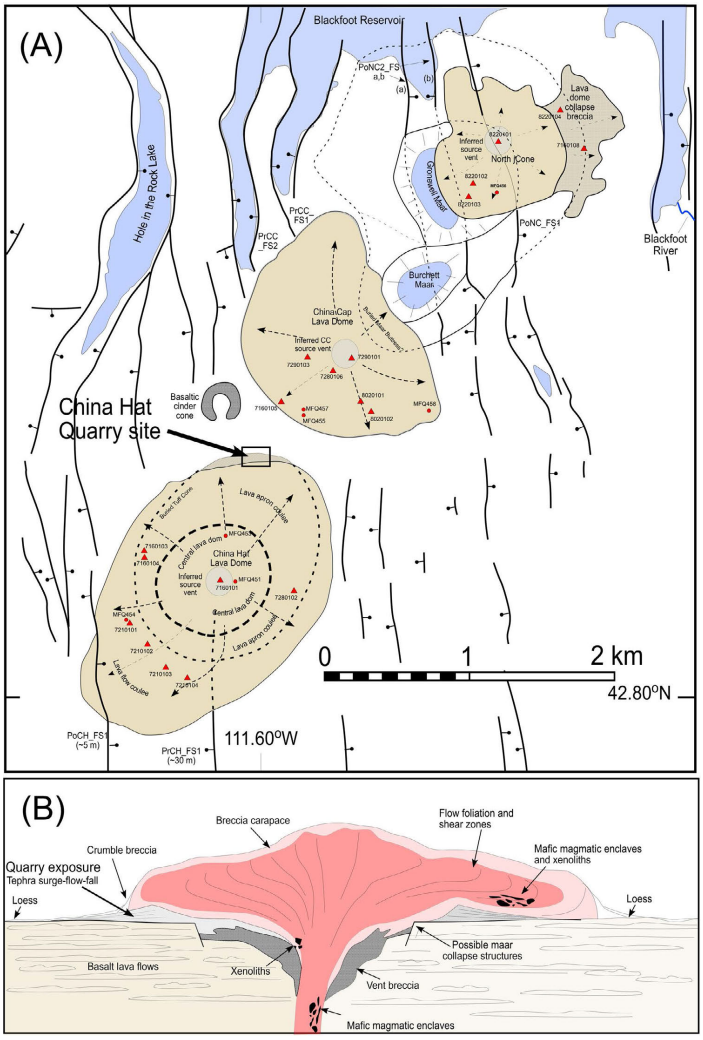

↑ **Figure 4.** (A) Simplified geologic map of the China Hat lava dome complex. The map illustrates sampling sites, inferred vents and dispersal patterns for the three lava domes and two cogenetic maars, and also the cross-cutting relationships between rift-related faults and the volcanic deposits. Importantly, it is apparent that faulting both pre- and post-dates formation of the rhyolite lava domes and maars. (B) Diagrammatic cross-section of the lava domes modified from Christiansen et al. (2007), illustrating inferred volcanic and hypabyssal intrusive facies of the lava dome complex.

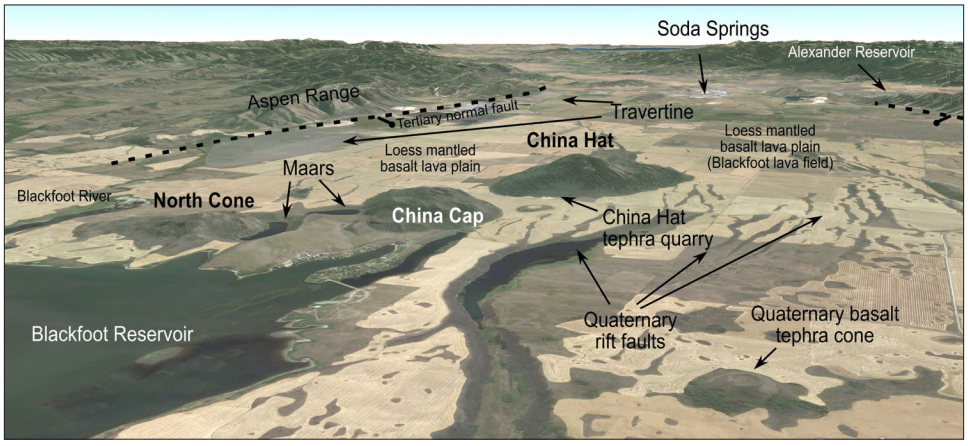

Figure 3. Overview of the China Hat lava dome and maar complex. This is a Google map image of the area as viewed from an elevation of ~5 km, looking to the south. The image illustrates key tectonic and volcanic features of the volcanic field. Tertiary normal faults bound the Aspen Range (on the east) and Soda Springs Hills and Chesterfield Range (on the west) produced a Tertiary graben that infilled with silicic volcanics and sediments of the Salt Lake Formation, and up to 250 m of late Pliocene to late Pleistocene basalt lavas. Voluminous travertine deposits occur along the range bounding normal fault of the Aspen Range. Prominent late Pleistocene normal faults and monoclines of the 'Blackfoot Rift Zone' (Polun 2011) produce prominent scarps that cut basalts lavas and some of the basalt tephra cones.

1983). The southernmost and youngest cluster, the China Hat dome field(CHDF), includes three coeval and geochemically and mineralogically similar domes (China Hat, China Cap and North Dome, and two maars (Figure 4). Cumulative volume of the CHDF lavas is ~1 km^3 (Ford 2005; Heumann 1999). Heumann (1999; 2004) documents a $^{40}Ar/^{39}Ar$ age of 57±8 ka for the three domes, refining previous dates obtained by K/Ar and TL and hydration rind methods (Armstrong et al., 1975; Leeman and Gettings, 1977).

Figure 4(a) illustrates key aspects of the geology of the China Hat lava dome field. The map emphasizes inferred vents and dispersal patterns for the three lava domes and cogenetic maars. Figure 4(b) is a diagrammatic cross-section of the lava domes modified from Christiansen et al. (2007), that illustrates products of precursory phreatomagmatic phases of eruption, including formation of tephra cones and maars, followed by effusive eruption of rhyolite. Both phreatomagmatic and effusive rhyolite contains trace amounts of isolated and swarm-like aggregates of mafic magmatic enclaves (Goldsby, ISU MS Thesis, in progress).

Interestingly, the lava domes and maars are well aligned towards the northeast, deviating 60 degrees clockwise from most regional extensional structures, and roughly coincides with a S-like, right-stepping bend in the Blackfoot Rift Zone. The alignment of vents suggests vertical connection to a common dike-like source at depth, as suggested by Heumann (1999). Figure 4(a) also illustrates that the lava domes were emplaced into a rift-like system small normal faults and monocline. Basalt lavas are commonly overlain by a thin, discontinuous layer of loess (basalt and loess and undifferentiated; shown as white. Diachronous episodes of faulting are indicated by fault scarps that are overlain by the 57 ka rhyolite (e.g., PrCHFS1, Figure 4a) and others that cut the rhyolite (e.g., PoCHFS1, Figure 4a). Faulting appears to postdate most, if not all of the basalt lavas near China Hat.

Age relationships between basalt lavas and rhyolites are unclear because contacts are widely obscured by loess. A basalt located 10 km southeast of China Hat yielded a $^{40}Ar/^{39}Ar$ date of 1.08±0.08 (Pickett, 2004). However lavas and tephra cones in the Blackfoot lava field exhibit wide variation in erosional dissection, and have both normal and reverse paleomagnetic signatures (Mabey and Oriel 1970). Fiesinger et al. (1982) suggest that some basalt volcanism post-dates China Cap (their 'Middle Cone'). However we suggest that poorly exposed basalt on the north flank of the dome (along with rhyolite lithics and pumice), are very coarse phreatomagmatic ejected debris rather than lava flows. The lava domes therefore postdate adjacent basalt lavas.

Formation of the China Hat dome field initiated with strong phreatomagmatic activity leading to development of maars. North cone partially infills Gronewell Lake maar; limited exposures on the north sides of both China Hat and China Cap suggest that those domes were also preceded by phreatomagmatic activity and possible maar development, followed by effusion of the lava domes (Figure 4b). Effusive facies of the lava domes vary from massive to flow-banded. Lava domes are finely pumiceous to dense and glassy in along flow margins, and finely crystalline in flow interiors. Minor common vapor-phase minerals such as alkali feldspar

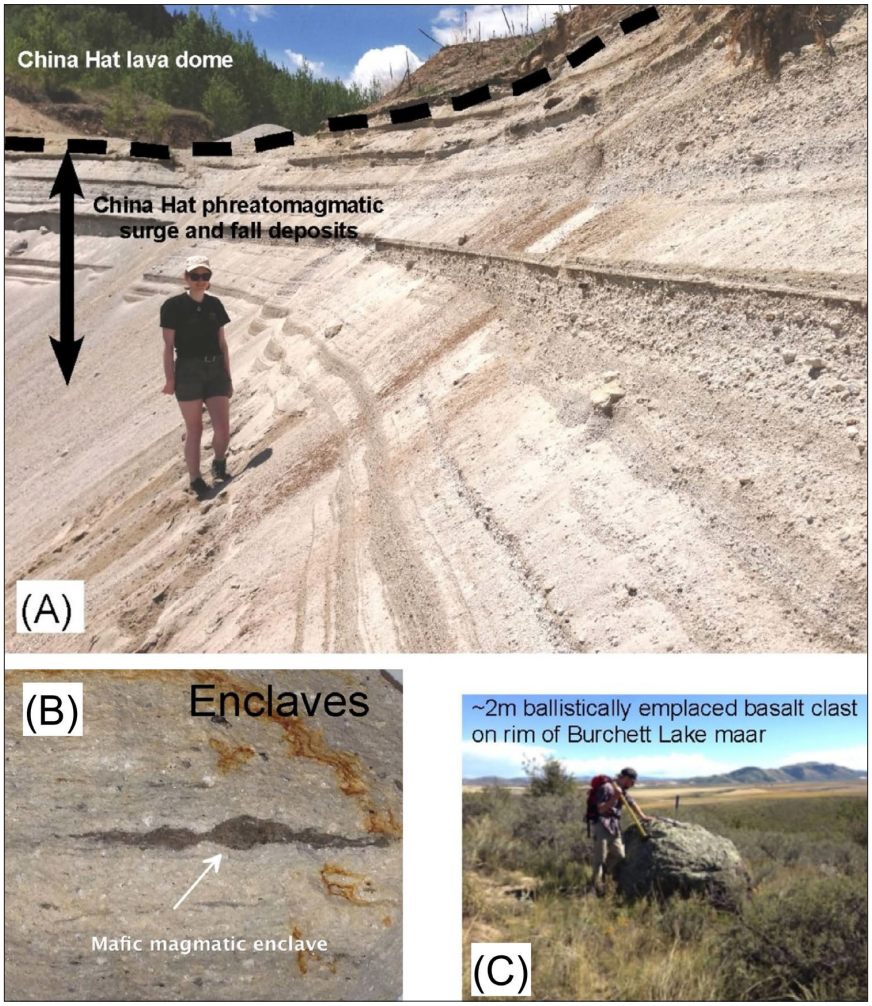

Figure 5. (A) Tephra quarry located on the north flank of China Hat. At this location the tephra deposits dip gently ~5 degrees the north, and are inferred to be medial facies of a tephra cone or maar that underlies China Hat. (B) A 5 cm long mafic magmatic enclave hosted in China Hat rhyolite. (C) Example of a ballistically emplaced block of basalt on the rim of Burchett Lake maar.

and quartz coat fractures and vesicles in some areas (Devault et al. 1984 document topaz in some of these), but there is no evidence for strong post-emplacement vapor-phase or hydrothermal alteration.

Total mass of pyroclastic rhyolite is estimated to less than a few percent of total erupted rhyolite volume. Best exposures occur in quarried rocks on the north flank of China Hat (Figure 5a). The quarry exposes ~8 meters (base not exposed) of gently north-dipping pyroclastic surge deposits. Clasts are dominated by well bedded, moderately well- to poorly sorted, weakly vesicular to dense essential rhyolite vitrophyre clasts and accidental basalt lithics. Some basalt lithics are weakly palagonitized. Unusually large, ballistically emplaced(?), basalt and rhyolite lithics are interspersed in the deposits. Basalt clasts up to 2 m diameter occur on the rim of Burchett maar (Figure 5c). Detailed petrographic and granulometric study of the China Hat quarry deposits indicates that only ~1% of rhyolite clasts have pumiceous textures. Mean lithic density is ~1.9 gm/cm^3, indicating low average vesicularity (Figure 5b). Additionally, all lithics, including pumices, have blocky morphology characteristic of fragmentation by sudden contraction during a fuel-coolant interaction when rising felsic magma encountered external water-rich country rocks near the surface. A 60±6 ka syngenetic layer of lapilli tuff occurs at a depth of 15.5 m at Grays Lake 20 km northeast of China Hat (Lageson et al. 1999), and attests to the strong exclusivity of some of the precursor eruptions of the lava domes. Nevertheless our work indicates that volatiles derived from the rhyolite magma played little role in that explosivity. Significantly, the absence of significant vesicularity in either pyroclastic or effusive parts of the China Hat lava domes, or other evidence of significant volatile degassing indicates that the original magmas arrived near the surface with a small fraction of H_2O required to crystallize the observed biotite autocrysts (cf. Westrich et al. 1988), or to account for high apparent H_2O contents of glass inclusions in autocrysts (Ford 2005).

Petrologic Context

Basalts and rhyolites of the BVF overlap in many of their petrologic and geochemical characteristics with coeval (Quaternary-Holocene) rocks of the ESRP (e.g., Manea et al. 2009; Leeman et al. 2009; McCurry et al. 2008; Shervais et al. 2006). Whole rock major element patterns and Nd- and Sr-isotope ratios are illustrated in Figure 6A and 6C. Most basalt are primitive olivine - plagioclase phyric olivine tholeiite, likely derived from Precambrian subcrustal, possibly

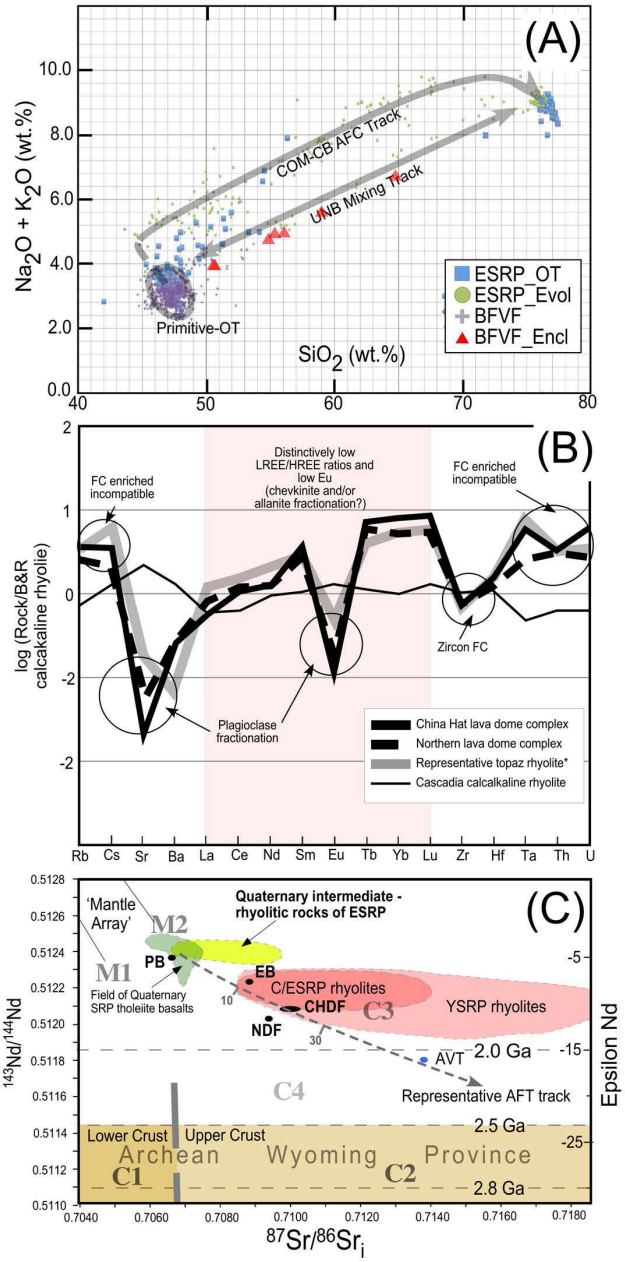

Figure 6. (A) TAS diagram illustrates the similarity in whole-rock major element chemistry between the mafic and felsic rocks of BVF and coeval rocks erupted on the Eastern Snake River Plain (Christiansen and McCurry 2008). ESRP_OT = olivine tholeiite basalt of Eastern Snake River Plain; ESRP_Evol = Quaternary evolved rocks of ESRP; BFVF=Blackfoot volcanic field; BFVF_Encl=mafic enclaves from China Hat and China Cap (Goldsby, personal communication, 2015). COM-CB AFC track and UNB mixing track are magma evolution pathways for Quaternary evolved rocks of ESRP (McCurry et al., 2008). (B) Spider diagram indicates the distinctive, topaz-rhyolite-like trace element characteristics of China Hat and other rhyolites of the BVF. These patterns are compared to much more voluminous calc-alkaline Neogene rhyolites of the Great Basin, and the Cascade volcanic arc (data from Christiansen and McCurry 2008). (C) Plot of Sr- and Nd-isotopic compositions of mafic and felsic rocks from BVF (data from Ford 2005; Pickett 2004; Heumann 1999; McCurry, unpublished data). PB – is a 'primitive olivine tholeiite', EB – is an isotopically evolved basalt. Representative fields are shown in black for samples from the Northern Dome Field (NDF) and China Hat Dome Field (CHDF). Colored fields illustrate fields for regionally significant rock types including rhyolites of the Yellowstone-Snake River Plain hot spot track (shades of red), Quaternary mafic and evolved rocks of the Eastern Snake River Plain (darker and lighter shades of green), and xenoliths and surface exposures of Archean mid- and lower-continental crust (lighter and darker shades of brown) (modified from McCurry and Rodgers 2009). M1, M2, C1-4 indicate the isotopic 'fingerprints' of plausible reservoirs that may have contributed mass to volcanic rocks of BVF (elaborated in Figure 7). Dashed arrowed line illustrates a plausible AFC (assimilation and fractional crystallization) pattern for primitive BVF basalt (PB); mass fraction of upper continental crust (reservoir C2) is shown as hash marks on the AFC line.

pyroxenite veined, spinel-lherzolite mantle. Deeper plume contributions are mainly transfers of heat and ^{3}He via a discrete fluid/gas phase (e.g., Manea et al. 2009). As in ESRP, there are lesser amounts of mafic, intermediate and felsic composition rocks that plot along simple mixing lines (UNB track) or in 'evolved' compositional regions. The latter could be produced either by extensive polybaric fractional crystallization of primitive olivine tholeiite ± assimilation (COM-CB AFC track) or by repeated fractional melting and intra-crustal recycling of Neogene mafic intrusive rocks (e.g., Shervais et al. 2006; Bindemann and Simakin 2014). Based upon limited sampling and analysis it appears that a higher fraction of basalts in BVF have undergone some degree of crustal interaction, indicated in more evolved isotopic compositions and presence of sodic plagioclase and ocellar quartz xenocrysts in many lavas (Fiesinger et al., 1982). Interestingly, Fiesinger et al. (1982) and Puchy (1981) also note the occurrence of rare olivine-augite basaltic trachyandesites. Fiesinger et al. (1982) infer that these lavas may be derived from distinctive mica-bearing peridotite mantle source, and attest to the possible high degree of complexity of mantle sources for the basalts.

Rhyolite lava domes of BVF are highly geochemically evolved 'topaz rhyolites' (e.g., Christiansen et al. 2006; Dayvault et al., 1984; Heumann 1999; Ford 2005). The lavas are silica and fluorine-rich (for China Hat, up to 77% and 0.6% respectively) and have high concentrations of incompatible trace elements (e.g., Rb, Cs, Ta, Th and U), low concentrations of compatible elements (TiO_2, MgO, P_2O_5), and distinctive trace element ratio signatures that are indicative of feldspar and accessory mineral fractionation (Figure 6b) (e.g., Heumann 1999; Ford 2005). Interestingly, Li-concentrations are high in China Hat (~100 ppm), even relative to other topaz rhyolites.

The China Hat lava dome field in particular contains a robust cargo of phenocrysts as well as some sparse occurrences of mafic magmatic enclaves (MME's). Ford (2005) estimates a phenocryst total of ~8% consisting of quartz> sanidine>plagioclase>hornblende≈biotite>magnetite>ilmenite and accessory zircon>apatite>thorite≈allanite. Dayvault et al. (1984) also report occurrence of epidote and other unidentified rare phases. Ford (2005) estimated pre-eruption magma crystallization conditions, based upon Fe-Ti oxide equlibria and amphibole thermobarometry, to be ~760°C and pressure corresponding to a depth of ~12-14 km. Reconnaissance U-series analyses of zircon phenocrysts (Heumann 1999; Schmitt 2011) indicate they crystallized within thousands of years of their eruption. Ongoing work on MME's by Goldsby (ISU MS Thesis, in progress) indicates mixing of olivine tholeiite and rhyolite. Additional work by Lochridge (ISU MS Thesis, in progress) and other collaborators is underway to interpret details of magma evolution as recorded by the robust assemblage of phenocrysts in the BLV topaz rhyolites, and by utilizing newly available quantitative modeling methods (cf. Bohrson et al., 2014).

BLV rhyolites are similar to Quaternary rhyolites of the ESRP, and they are interpreted to have evolved in similar fashion (e.g., McCurry et al., 2008; Ford 2005). However in contrast to Quaternary pyroxene±fayalite-bearing ESRP rhyolites, BVF rhyolites contain hydrous phenocrysts (biotite and hornblende). They also have slightly more evolved isotope ratios and high F-contents that are indicative of slightly greater degree of assimilation of Archean granitic upper crust (e.g., Ford 2005).

Conceptual Models

Regional BVF Model

Figure 7a illustrates a simplified and diagrammatic cross-sectional conceptual model for the large-scale architecture of the BLV. Mantle and crust are subdivided into potentially disguishable mass reservoirs. The ultimate heat and mass reservoir is illustrated as reservoir M1 (deep mantle). This region is modeled as derived by roll-over of deep mantle plume material produced by ongoing, but waning vertical convection beneath ESRP (e.g., Humphreys et al. 2000). Following Manea et al. (2009) we infer that this layer mainly contributes a flux of high 3He fluids and heat to the Precambrian subcrustal upper mantle (SCUM = M2). Both fluxes are inferred to decline in magnitude away from the axis of ESRP (dashed line in inset figure). Alternately, spatial variability in melt production may be derived from passive response of more- and less-fertile regions upper mantle to regional extension (e.g., Manea et al. 2009).

Layer M2 (subcrustal upper mantle) is modeled as dominated by depleted, isotopically evolved (EM1-EM2 type) Archean peridotite. M2 is inferred to be the single most important source of mass and heat for the BVF. Significant heterogeneity of M2 is expected and, as suggest by Manea et al. (2009), may play a fundamental role in magma productivity, and should be tested in future work (Manea et al. 2009; Leeman, personal communication, 2014). However at present the degree and scale of heterogeneity is unconstrained. In this model we infer that the effects of heterogeneity on magma productivity are muted by vertical mixing and hybridization processes leading to consistent rates of segregation of primitive olivine tholeiite and/or picrite above the garnet-spinel transition zone (<70-100 km), and buoyant transfer of that melt to the Moho and shallower crustal depths. Occurrence of partial melt at the Moho has been suggest by Peng and Humphreys (1998). Flux of mantle-derived melt into the crust is unknown. Approximately 100 km3 of basalt have been erupted in the last ~2 Ma in the BVF. Making the speculative assumption that half the magma transferred to the crust is erupted leads to a magma transfer rate of ~0.1 km^3/1000 yr.

Crustal architecture is divided into four reservoirs (McCurry and Rodgers 2009; DeNosaquo et al. 2009; Yuan et al. 2010; and references therein). Lower and upper crustal layers C1 and C2 are modeled as Archean, Wyoming craton-type crystalline rocks, having geochemical tracer characteristics outlined in Figures 7a and 6c. As in the case of the upper mantle, for lack of constraints, we assume that the effects of crustal heterogeneities are muted at the scale of the BVF magmatic system. Layer C3 is modeled as Proterozoic to Mesozoic Miogeoclinal sedimentary rocks that have been shingled together via Sevier thrust faults to a thickness of 8 to 10 km. We suggest that these rocks mainly play a role of density, and possible structural trap for ascending magmas. Layer C4 is a layer of dense rocks that was produced by MASH and AFC-type processes along the YSRP (e.g., Christiansen and McCurry 2008; Annen et al. 2009). Those dense rocks collapsed isostatically from beneath ESRP via ductile lower crustal flow into regions marginal to the YSRP during culmination of hot spot track activity between ~10 and 4.5 Ma (e.g., Rodgers and McCurry 2009; Yuan et al. 2010). This lower crustal flow may extend as far from ESRP as BVF (DeNosaquo et al. 2009). Christiansen and McCurry (2008) and McCurry and Rodgers (2009) model this layer as having and average diorite-like bulk composition, and consisting of partial melting restite and masses of unmelted upper crust riddled by gabbroic dikes and sills. In our conceptual model layers C1 and C4 are refractory, and dense enough to support buoyant transfer of primitive magmas to the boundary of layers C1 and C2, where crustal density drops 10%. We speculate that vertical transfer of magma is opportunistic, and focused by space availability resulting from oblique extension.

By analogy with Quaternary bimodal volcanism in ESRP (McCurry et al. 2008; Whitaker et al. 2008; Shervais et al. 2006; Bindeman and Simkin 2014) production of evolved magma compositions occur primarily via MASH and polybaric FC (Figure 7b), while magma mixing and cyclic remelting play subsidiary roles. Magma evolution culminates incrementally and unsteadily with collection and storage lesser, and more transient but still significant volumes of highly evolved, China-Hat-like rhyolitic magma near the contact between layers C2 and C3.

China Hat Model

Figures 7 and 8 illustrate what we propose to be an evolving plutonic and magma storage and processing system beneath central parts of the BVF. Upper parts of that system are emphasized in Figure 8 and are inferred to be dominantly felsic in composition. Leeman and Gettings (1977) interpret gravity and magnetic anomalies in the China Hat area and petrologic data from the volcanic rocks as suggesting that a hot silicic laccolith having a volume of up 330 km^3 underlies the China Hat lava dome field at between 0.5 and 6 km depth. The Blackfoot Rift Zone could accommodate a volume

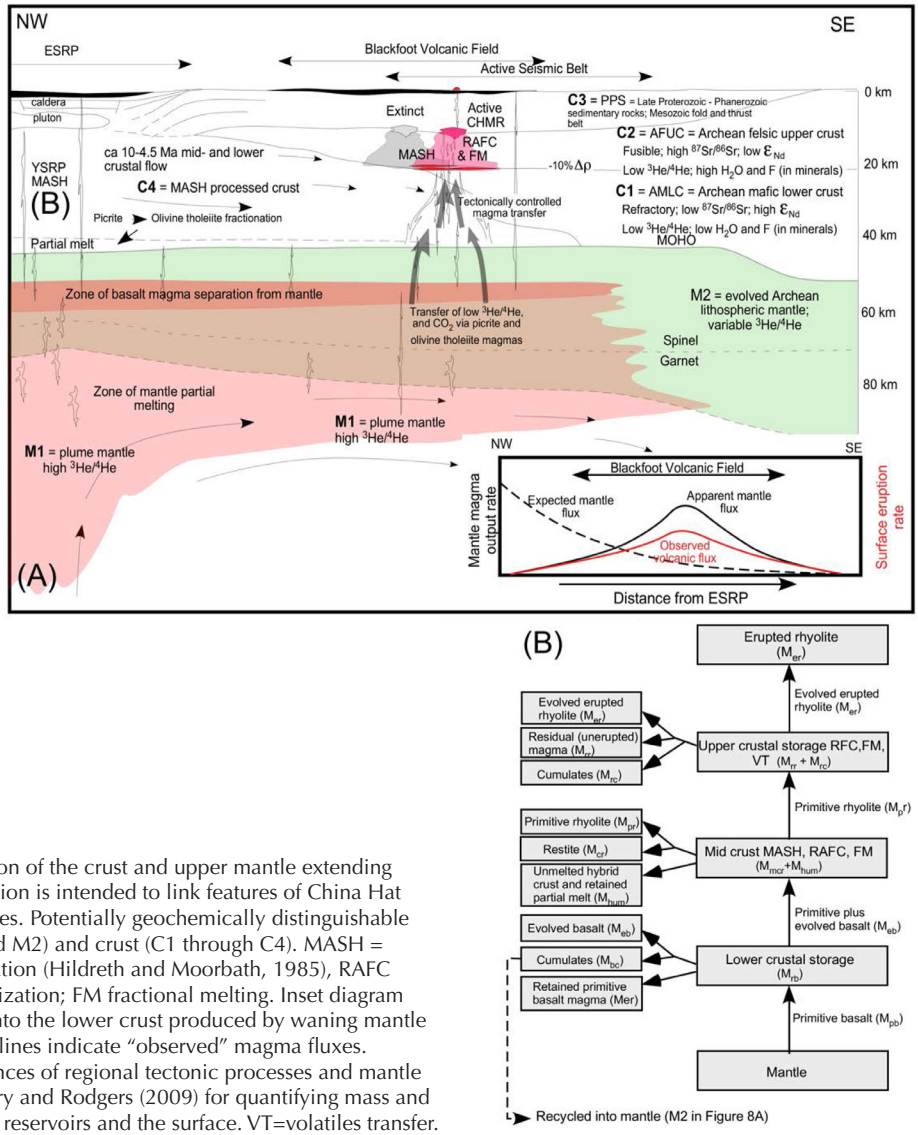

Figure 7. (A) Diagrammatic NW-SE cross-section of the crust and upper mantle extending SE from the YSRP hot spot track. The cross-section is intended to link features of China Hat and BVF to its underlying mass and heat sources. Potentially geochemically distinguishable reservoirs are indicated for the Mantle (M1 and M2) and crust (C1 through C4). MASH = melting, assimilation, storage and homogenization (Hildreth and Moorbath, 1985), RAFC = recharge, assimilation and fractional crystallization; FM fractional melting. Inset diagram illustrates a hypothetical mantle magma flux into the lower crust produced by waning mantle convection (dashed line). Red and black solid lines indicate "observed" magma fluxes. Differences are inferred to reflect the significances of regional tectonic processes and mantle fertility. (B) A flow chart modified from McCurry and Rodgers (2009) for quantifying mass and energy exchanges between mantle and crustal reservoirs and the surface. VT=volatiles transfer.

0 to at least 20 km^3 of intrusive rocks in the upper 10 km of crust; the higher value assumes the the rift system is dike induced (Polun 2010). Cumulative silicic magma transfer to the surface or hypabyssal intrusions is therefore estimated to be between 1.2 and 350 km^3. Deeper parts of the system are inferred to be dominated by less evolved, more mafic plutonic rocks, restite, cumulates and unmelted upper crust.

Thermobarometry work by Ford (2005) indicates pre-eruptive crystallization (i.e. storage) of the China Hat rhyolite occurred at 12-14 km depth, and very close to the contact between Miogeoclinal sedimentary rocks and Archean upper crust. As pointed out by Autenreith et al. (2011), McCurry and Welhan (2012) and Welhan et al. (2014) it also coincides with intersections of major Sevier-age thrust faults. We suggest that vertical changes in crustal density coinciding with older structures in that region could combine with space accommodation provided by tectonic extension to produce a favorable environment for magma accumulation in the middle crust.

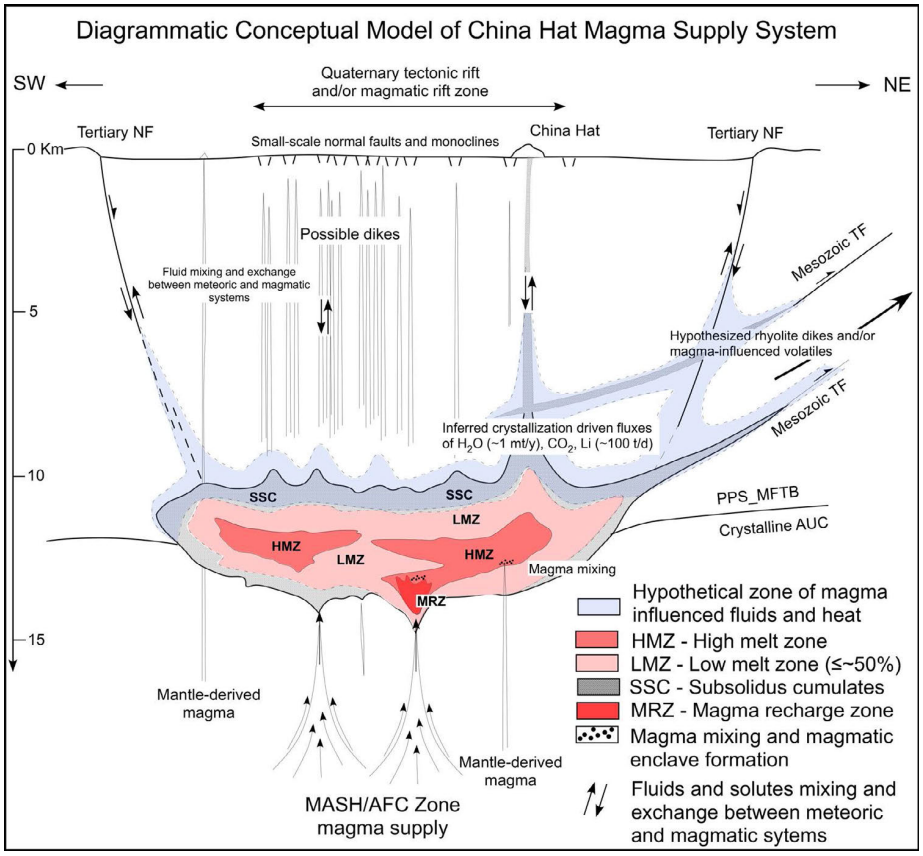

Figure 8. A diagrammatic conceptual model for China Hat and the BVF. This model is not to scale, but it highlights plausible features and processes of the uppermost, geochemically evolved parts of the inferred magmatic and hydrothermal systems. CHMR = China Hat magma reservoir and pluton system.

Our model emphasizes that the shallow parts of the magmatic system grow incrementally and are highly variable in melt content and fluctuate over time and space. It is likely that no more than a small fraction of the pluton contains 'eruptible magma' at a particular time (e.g., Bachmann et al. 2007). Magma inputs are dominantly from mid-crustal melt zones, but also include intrusions of mantle-derived basalt. Those basalts likely contribute significantly to the energy balance and He- and C-isotope characteristics of the magma reservoir system. High melt zones wax and wane in volume and location over time owing to recharge, volatile evolution and rate of heat loss to the surroundings.

Melts generated in the mid-crust via MASH inherit significant H_2O and fluorine from Archean upper crust via crustal anatexis. These volatiles and incompatible trace element concentrations increase via extreme fractional crystallization, eventually leading to saturation in amphibole and biotite micas ($H_2O \geq$ ~4% based on presence of biotite and low EMP totals for quartz-hosted melt inclusions). We infer that crystallization of volatile rich magma in shallow parts of the reservoir system occurs rapidly enough so that exsolved volatiles and volatile-soluble trace elements escape into the surroundings. Additionally. we speculate that preferred volatile pathways follow pre-existing high permeability zones that likely include thrust faults and young normal faults, perhaps channeling fluids into regions laterally distant from their source (e.g., Welhan et al. 2014).

Implications

If a silicic pluton and related magma storage system is developing beneath the China Hat region, as we suggest, it would produce significant thermal, volatiles and volatile-soluble constituent fluxes into the surroundings. As a working hypothesis, H_2O and CO_2 fluxes are estimated given the following simplistic, but plausible assumptions:

1. magma production rate is constant and can be averaged over life-span of BVF (estimated to be ~2 m.y.);
2. total rhyolite output is between 1.2 and 350 km^3;
3. all surficial and hypabyssal rocks are the same type as China Hat;
4. magmas had an initial water content of 2-5 wt.%;
5. all water is lost to surroundings during crystallization and that crystalline material is anhydrous (or nearly so);
6. the intrusion/'extrusion' (including hypabyssal intrusions) ratio is approximately 5:1.

Figure 9 illustrates a derived range of H_2O and CO_2 volatile flux from the China Hat Magma Reservoir system of 0.1 and 100 MT/yr H_2O and 10 to 1000 t/day CO_2. Interestingly, Lewicki et al. (2013) estimated a 'deeply derived' CO_2 flux of ~350 t/day from springs systems ~10 km south of China Hat.

Owing to the high concentrations of incompatible elements in topaz rhyolites, and strong fractionation of some of those elements into the aqueous phase during magma degassing, we speculate that some may be traceable into depths accessible in boreholes, or even in groundwater and springs. For example, Hofstra et al. (2013) demonstrate the connection between Li-degassing of topaz rhyolites and transfer to shallow aquifer systems. China Hat rhyolite has whole-rock Li-concentrations comparable to or greater than those examined by Hofstra and coauthors, and may therefore have mass transfer rates comparable to the calculated CO_2 flux. Notably, Welhan et al. (2014) suggest that high Li-concentrations in deep borehole brines from the Greys Lake region, ~20 northeast of China Hat, may have been derived from the topaz rhyolite magma system. This idea is speculative, but if it is confirmed, it would both support the hypothesis that China Hat is a blind resource, and that the resource may be traceable.

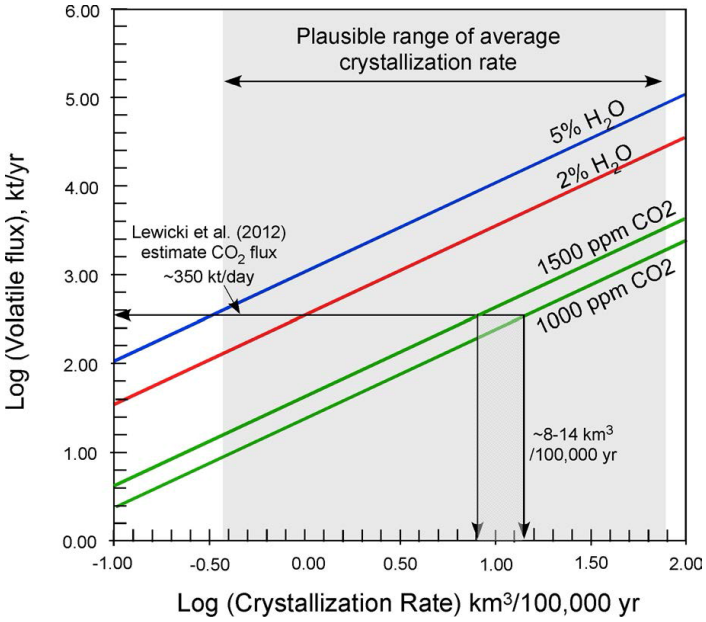

Figure 9. This figure illustrates plausible ranges of H_2O and CO_2 mass flux transferred from crystallizing parts of the China Hat magma reservoir into the upper crust.

Conclusions and Future Work

We present an improved conceptual model and quantitative framework for testing links between magmatic-related heat sources and shallower geothermal systems at the Blackfoot Volcanic Field. We suggest that the field has developed owing to opportunistic interaction between evolving tectonic transtensional processes and mantle convection driven partial melting. Ongoing extension and magmatism likely reflect development of a dynamic mid- to upper crustal plutonic and magma storage system. Rates of silicic magma production are ~1 to 200 km^3/m.y. H_2O and CO_2 volatile fluxes from the rhyolite source region of ~0.1 to 10 MT/year and 10 to 1000 T/day, respectively. Lithium flux may be comparable to CO_2, and it may be both an effective tracer and resource in fluids derived from the inferred consolidating China Hat magma body.

There is considerable potential for additional exploration of the China Hat region as a blind geothermal resource. Future work should better characterize the timing of slip along range-bounding and basin-centered structures and the relationship to magma generation, normal fault geometries in map view and in the subsurface, and the potential role of basement heterogeneities in controlling slip transfer to northwest-striking structures in east-central Idaho. Better resolution of local seismicity and deep conductivity could help resolve existence of upper crustal magmas and related hot brine solutions. Exploiting the rich phenocryst cargo and enclaves in China Hat-related rhyolites would better define magma genesis, upper crustal storage frequency/flux, and geochemical tracer source characteristics. Additional dating and geochemical analyses of basalts is needed to evaluate a possible southward, time-transgressive focus of magmatism. Voluminous travertine deposits, particularly those bordering the Aspen Range, may contain a Pleistocene to Holocene record of magmatic-associated tracer chemistry. Examination of deep borehole core from regions of high heat flow northeast of China Hat is needed for indications of hydrothermal alteration and possible connection to China Hat-derived fluids.

Acknowledgements

We recognize and greatly appreciate numerous discussions, support, and other contributions from colleagues (Dave Rodgers, Suzette Payne, Bill Leeman, Hana Nekvasil, Bill Bonnichsen, Travis McLing, Scott Hughes, Mitch Plummer, Axel Schmitt), and students, including Mark Ford, Kate Pickett, Sean Polun, Rebecca Ohly, Bill Lochridge and Ryan Goldsby. We also thank Clay Cooper for a review of the paper.

References

Arehart, G.B., Coolbaugh, M.F., and Poulson, S.R., 2002, Geochemical characterization of geothermal systems in the Great Basin: Implications for exploration, exploitation, and environmental issues: Transactions-Geothermal Resources Council, p. 479–482.

Armstrong, R.L., Leeman, W.P., and Malde, H.E., 1975, K-Ar dating, Quaternary and Neogene volcanic rocks of the Snake River Plain, Idaho: American Journal of Science, v. 275, p. 225–251, doi: 10.2475/ajs.275.3.225.

Autenrieth, K.D., McCurry, M., Welhan, J., and Polun, S., 2011, Conceptual Subsurface Model of the Blackfoot Volcanic Field , Southeast Idaho: A Potential Hidden Geothermal Resource: GRC Transactions Vol 35, v. 35, p. 695–698.

Bachmann, O., and Bergantz, G.W., 2008, Rhyolites and their source mushes across tectonic settings: Journal of Petrology, v. 49, p. 2277–2285.

Bachmann, O., Miller, C.F., and de Silva, S.L., 2007, The volcanic–plutonic connection as a stage for understanding crustal magmatism: Journal of Volcanology and Geothermal Research, v. 167, p. 1–23.

Bindeman, I.N., and Simakin, A.G., 2014, Rhyolites — Hard to produce , but easy to recycle and sequester : Integrating microgeochemical observations and numerical models: Geosphere, v. 10, p. 930–957.

Bohrson, W. a., Spera, F.J., Ghiorso, M.S., Brown, G. a., Creamer, J.B., and Mayfield, a., 2014, Thermodynamic Model for Energy-Constrained Open-System Evolution of Crustal Magma Bodies Undergoing Simultaneous Recharge, Assimilation and Crystallization: the Magma Chamber Simulator: Journal of Petrology, v. 55, p. 1685–1717.

Breckenridge, RM, Lewis, RS, Adema, GW and Weisz, DW, 2003, Miocene and younger faults in Idaho. Geological Society of America Memoir 179, p. 1-53.

Byrd, J.O.D., Smith, R.B., and Geissman, J.W., 1994, The Teton fault, Wyoming: Topographic signature, neotectonics, and mechanisms of deformation: Journal of Geophyscial Research, v. 99, p. 20095–20122.

Christiansen, E.H., Sheridan, M.F., and Burt, D.M., 1986, The geology and geochemistry of Cenozoic topaz rhyolites from the western United States: Geological Society of America Special Paper, v. 205, 82 p.

Christiansen, E.H., Haapala, I., and Hart, G.L., 2007, Are Cenozoic topaz rhyolites the erupted equivalents of Proterozoic rapakivi granites? Examples from the western United States and Finland: Lithos, v. 97, p. 219–246.

Christiansen, E.H., and McCurry, M., 2008, Contrasting origins of Cenozoic silicic volcanic rocks from the western Cordillera of the United States: Bulletin of Volcanology, v. 70, p. 251–267.

Dayvault, R.D., Rush, S.M., and Ludlam, J.R., 1984, Reports on field investigations of uranium anomalies - Part II. Evaluation of uranium potential in topaz-bearing rhyolite, China Hat Dome, southeastern Idaho: Bendix Field Engineering Corporation Report GJBX-1(84) for US DOE.

DeNosaquo, K.R., Smith, R.B., and Lowry, A.R., 2009, Density and lithospheric strength models of the Yellowstone-Snake River Plain volcanic system from gravity and heat flow data: Journal of Volcanology and Geothermal Research, v. 188, p. 108–127.

Dixon, S., 1982, Regional structural synthesis, Wyoming Salient of Western Overthrust Belt: AAPG Bulletin, v. 66, p. 1560–1580.

Faulds, J.E., and Henry, C.D., 2008, Tectonic influences on the spatial and temporal evolution of the Walker Lane: An incipient transform fault along the evolving Pacific–North American plate boundary: Arizona Geological Society Digest, v. 22, p. 437–470.

Faulds, J.E., Hinz, N.H., Coolbaugh, M.F., Cashman, P.H., Kratt, C., Dering, G., Edwards, J., Mayhew, B., and Mclachlan, H., 2011, Assessment of Favorable Structural Settings of Geothermal Systems in the Great Basin , Western USA: Geothermal Resource Council Transactions, v. 35, p. 777–793.

Fiesinger, D.W., Perkins, W.D., and Puchy, B.J., 1982, Mineralogy and petrology of Tertiary-Quaternary volcanic rocks in Caribou County, Idaho, *in* Bonnichsen, B. and Breckenridge, R.M.. eds., Cenozoic Geology of Idaho, Idaho Bureau of Mines and Geology Bulletin 26, p. 465–488.

Ford, M.T., 2005, The petrogenesis of Quaternary rhyolite domes in the bimodal Blackfoot Volcanic Field: Idaho State University, 133 p.

Grant, J. V., and Kattenhorn, S. A., 2004, Evolution of vertical faults at an extensional plate boundary, southwest Iceland: Journal of Structural Geology, v. 26, p. 537–557.

Heumann, A., 2004, Timescales of evolved magma generation at Blackfoot Lava Field , SE Idaho , USA: Abstract for International Association of Volcanology and Chemisty of the Earth's Interior (IAVCEI) General Assembly, Volcanism and its impacts on society, Pucon, Chile (http://www.iavcei.org/documents/pucon04/pucon04abs.html).

Heumann, A., 1999, Timescales of processes within silicic magma chambers: PhD Dissertation, University Amsterdam, 200 p.

Hofstra, a. H., Todorov, T.I., Mercer, C.N., Adams, D.T., and Marsh, E.E., 2013, Silicate melt inclusion evidence for extreme pre-eruptive enrichment and post-eruptive depletion of lithium in silicic volcanic rocks of the Western United States: Implications for the origin of Lithium-Rich Brines: Economic Geology, v. 108, p. 1691–1701.

Humphreys, E.D., Dueker, K.G., Schutt, D.L., and Smith, R.B., 2000, Beneath Yellowstone: Evaluating plume and nonplume models using teleseismic images of the upper mantle: GSA Today, v. 10, p. 1–7.

Hutsinpiller, A., and Parry, W.T., 1985, Geochemistry and geothermometry of spring water from the Blackfoot Reservoir region, southeastern Idaho: Journal of Volcanology and Geothermal Research, v. 26, p. 275–296.

Lageson, D.R., Adams, D.C., Morgan, L., Pierce, K.L., and Smith, R.B., 1999, Neogene-Quaternary tectonics and volcanism of southern Jackson Hole, Wyoming and southeastern Idaho, *in* Hughes, S.S. and Thackray, G.D. eds., Guidebook to the Geology of Eastern Idaho, Idaho Museum of Natural History, p. 115–130.

Laumonier, M., Scaillet, B., Pichavant, M., Champallier, R., Andujar, J., and Arbaret, L., 2014, On the conditions of magma mixing and its bearing on andesite production in the crust: Nature Communications, v. 5, p. 5607, doi: 10.1038/ncomms6607.

Leeman, W.P., and Gettings, M.E., 1977, Holocene rhyolite in SE Idaho and geothermal potential: EOS, American Geophysical Union, v. 58, p. 1249.

Leeman, W.P., Schutt, D.L., and Hughes, S.S., 2009, Thermal structure beneath the Snake River Plain: Implications for the Yellowstone hotspot: Journal of Volcanology and Geothermal Research, v. 188, p. 57–67, doi: 10.1016/j.jvolgeores.2009.01.034.

Lewicki, J.L., Hilley, G.E., Dobeck, L., McLing, T.L., Kennedy, B.M., Bill, M., and Marino, B.D.V., 2013, Geologic CO2 input into groundwater and the atmosphere, Soda Springs, ID, USA: Chemical Geology, v. 339, p. 61–70, doi: 10.1016/j.chemgeo.2012.06.013.

Luedke, R.G., and Smith, R.L., 1983, Map showing distribution, composition, and age of late Cenozoic volcanic centers in Idaho, Western Montana, West-Central South Dakota, and Northwestern Wyoming: U.S. Geological Survey Misc. Inv. Series Map I-1091-E

Mabey, D., and Oriel, S., 1970, Gravity and magnetic anomalies in the Soda Springs Region, Southeastern Idaho: U.S. Geological Survey Proffesional Paper 646-E.

Manea, V.C., Manea, M., Leeman, W.P., and Schutt, D.L., 2009, The influence of plume head–lithosphere interaction on magmatism associated with the Yellowstone hotspot track: Journal of Volcanology and Geothermal Research, v. 188, p. 68–85.

McCurry, M., Christiansen, E.H., and Leeman, W.P., 2007, Petrogenesis and volcanology of anorogenic rhyolites: a special issue dedicated to Bill Bonnichsen: Bulletin of Volcanology, v. 70, p. 247–249.

McCurry, M., Hayden, K.P., Morse, L.H., and Mertzman, S., 2008, Genesis of post-hotspot, A-type rhyolite of the Eastern Snake River Plain volcanic field by extreme fractional crystallization of olivine tholeiite: Bulletin of Volcanology, v. 70, p. 361–383.

McCurry, M., and Rodgers, D.W., 2009, Mass transfer along the Yellowstone hotspot track I: Petrologic constraints on the volume of mantle-derived magma: Journal of Volcanology and Geothermal Research, v. 188, p. 86–98.

McCurry, M., and Welhan, J., 2012, Do Magmatic-Related Geothermal Energy Resources Exist in Southeast Idaho ? GRC Transactions, v. 36, p. 699–707.

McCurry, M., Welhan, J., Polun, S., and Autenrieth, K., 2011, Geothermal Potential of the Blackfoot Reservoir-Soda Springs Volcanic Field : A Hidden Geothermal Resource and Natural Laboratory in SE Idaho Idaho Geological Survey , University of Idaho Geology and Hydrogeology: Geothermal Resource Council Transactions, v. 35, p. 917–924.

McLing, T.L., McCurry, M., Cannon, C., Wood, T., Neupane, G., Podgorney, R., Welhan, J., Mines, G., Plummer, M., Moore, J., Fairley, J., Wood, R., and Mattson, E., 2014, David Blackwell's Forty Years in the Idaho Desert, the Foundation for 21st Century Geothermal Research: GRC Transactions v. 38, p. 143-153.

Mitchell, J.C., 1976, Geochemistry and geologic setting of the thermal and mineral waters of the Blackfoot Reservoir area, Caribou County, Idaho:.

Moore, J, Enhanced geothermal systems – Concept testing and development at the Raft River Geothermal Field. DOE GTE Project Number EE0000215, 2009-2014, https://www4.eere.energy.gov/geothermal/projects/125, accessed April 2015.

Neely, K., and Galinato, G., 2007, Geothermal power generation in Idaho: An overview of current developments and future potential:.

Newman, S., and Lowenstern, J.B., 2002, Volatile Calc : a silicate melt – H2O – CO2 solution model written in Visual Basic for excel: Computers & Geosciences, v. 28, p. 597–604, doi: doi:10.1016/S0098-3004(01)00081-4.

Payne, S.J., McCaffrey, R., King, R.W., and Kattenhorn, S. A., 2012, A new interpretation of deformation rates in the Snake River Plain and adjacent basin and range regions based on GPS measurements: Geophysical Journal International, v. 189, p. 101–122.

Peng, X., and Humphreys, E.D., 1998, Crustal velocity structure across the easteru Snake River Plain and the Yellowstone swell: Journal of Geophyscial Research, v. 103, p. 7171–7186.

Pickett, K.E., 2004, Physical Volcanology , Petrography , and Geochemistry of Basalts in the Bimodal Blackfoot Volcanic Field , Southeastern Idaho By: Idaho State University, 92 p.

Pierce, K.L., and Morgan, L. a., 2009, Is the track of the Yellowstone hotspot driven by a deep mantle plume? — Review of volcanism, faulting, and uplift in light of new data: Journal of Volcanology and Geothermal Research, v. 188, p. 1–25, doi: 10.1016/j.jvolgeores.2009.07.009.

Podgorney, R., Mccurry, M., Wood, T., Mcling, T., Ghassemi, A., Welhan, J., Mines, G., Plummer, M., Moore, J., Fairley, J., and Wood, R., 2013, Enhanced Geothermal System Potential for Sites on the Eastern Snake River Plain, Idaho: GRC Transactions Vol 37, v. 37, p. 191–197.

Polun, S.G., 2011, Kinematic analysis of Late Pleistocene faulting in the Blackfoot Lava Field, Caribou County, Idaho: Idaho State University, 86 p.

Puchy, BJ, 1981, Mineralogy and petrology of lava flows (Tertiary-Quaternary) in southeastern Idaho and at Black Mountain, Rich County, Utah. University of Utah M.S. Thesis, 73 p.

Rodgers, D., Ore, H., and Bobo, R., 2002, Extension and subsidence of the eastern Snake River Plain, Idaho, *in* Bonnichsen, B., White, C., and McCurry, M. eds., Tectonic and Magmatic Evoluiton of the Snake River Plain Volcanic Province, Idaho Geological Survey Bulletin, p. 121–155.

Rodgers, D.W., and McCurry, M., 2009, Mass transfer along the Yellowstone hotspot track II: Kinematic constraints on the volume of mantle-derived magma: Journal of Volcanology and Geothermal Research, v. 188, p. 99–107.

Royse, J., Warner, M.A., and Reese, D.L., 1975, Thrust belt structural geometry and related stratigraphic problems Wyoming-Idaho-Northern Utah, *in* Symposium on Deep Drilling Frontiers in the Central Rocky Mountains, Rocky Mountain Association of Geologists, p. 41.

Schmitt, A.K., 2011, Uranium Series Accessory Crystal Dating of Magmatic Processes: Annual Review of Earth and Planetary Sciences, v. 39, p. 321–349.

Shervais, J.W., Vetter, S.K., and Hanan, B.B., 2006, Layered mafic sill complex beneath the eastern Snake River Plain: Evidence from cyclic geochemical variations in basalt: Geology, v. 34, p. 365–368.

Simakin, A.G., and Ghassemi, A., 2007, The mechanics of a magma chamber-fault system in trans-tension with application to Coso: Journal of Structural Geology, v. 29, p. 1971–1983.

Smith, R.B., and Sbar, M.L., 1974, Contemporary Tectonics and Seismicity of the Western United States with Emphasis on the Intermountain Seismic Belt: Geological Society of America Bulletin, v. 85, no. 8, p. 1205–1218.

Tester, J.W., Anderson, B.J., Batchelor, A.S., Blackwell, D.D., DiPippo, R., Drake, E.M., Garnish, J., Livesay, B., Moore, M.C., Nichols, K., Petty, S., Nichols, K., Petty, S., Toksoz, M.N., et al., 2006, The Future of Geothermal Energy. INL/EXT-06-11746 Report for USDOE (http://mitei.mit.edu/system/files/geothermal-energy-full.pdf)

Welhan, J., Gwynn, M., Payne, S., McCurry, M., Plummer, M., and Wood, T., 2014, The Blackfoot Volcanic Field , Southeast Idaho : A Hidden High-Temperature Geothermal Resource in the Idaho Thrust Belt: Proceedings Ninth Workshop Geothermal Reservoir Engineering Stanford University, Stanford, California, February 24-26, 2014, v. SGP-TR-202, p. 1–13.

Westrich, H.R., Stockman, H.W., and Eichelberger, J.C., 1988, Degassing of rhyolitic magma during ascent and emplacement: Journal of Geophysical Research, v. 93, p. 6503-6511.

Whitaker, M.L., Nekvasil, H., Lindsley, D.H., and McCurry, M., 2008, Can crystallization of olivine tholeiite give rise to potassic rhyolites? - An experimental investigation: Bulletin of Volcanology, v. 70, p. 417–434.

Yuan, H., Dueker, K., and Stachnik, J., 2010, Crustal structure and thickness along the Yellowstone hot spot track: Evidence for lower crustal outflow from beneath the eastern Snake River Plain: Geochemistry, Geophysics, Geosystems, v. 11, 14 p.